

NTIS HC # 3-50

X-660-73-14

PREPRINT

NASA TM-X-66165

NUCLEAR GAMMA RAYS FROM SOLAR FLARES

(NASA-TM-X-66165)	NUCLEAR GAMMA RAYS	N73-16797
FROM SOLAR FLARES (NASA)	29 p HC \$3.50	
	CSSL 03B	
		Unclas
		G3/29 54121

R. RAMATY
R. E. LINGENFELTER

JANUARY 1973



GODDARD SPACE FLIGHT CENTER
GREENBELT, MARYLAND

NUCLEAR GAMMA RAYS FROM SOLAR FLARES

R. Ramaty
Laboratory for High Energy Astrophysics
NASA/Goddard Space Flight Center
Greenbelt, Maryland 20771

and

R. E. Lingenfelter
Institute of Geophysics and Planetary Physics and
Department of Planetary and Space Science
University of California, Los Angeles

ABSTRACT

The theory of gamma ray line emission from solar flares is reviewed and revised. It is shown that the recently observed (Chupp et al., 1972) line emissions at 0.5, 2.2, 4.4 and 6.1 MeV are due to positron annihilation, deuterium de-excitation following neutron capture on hydrogen, and the deexcitation of excited states in carbon and oxygen. From the observed relative line intensities it is possible to determine the spectrum of accelerated protons in the flare region. This spectrum is found to be very similar to that of charged particles from the flare observed near earth. The total numbers of protons at the sun is deduced from the observed absolute line intensities for various interaction models. It is found that if the protons at the sun have a spectrum which is an exponential in rigidity, the total energy in protons is a few times 10^{28} ergs if the gamma rays are produced by protons moving down into the sun; and about 10^{30} ergs if the gamma rays are produced at the site of the acceleration.

INTRODUCTION

Solar gamma-ray line emissions at 0.5, 2.2, 4.4 and 6.1 MeV were detected during the flare of August 4, 1972 by a gamma-ray monitor flown on OSO-7 (Chupp et al. 1972). Line emissions at 0.5 and 2.2 MeV were also detected on August 7, 1972, but only upper limits could be set on the 4.4 and 6.1 MeV lines from this flare. In previous papers (Lingenfelter and Ramaty 1967, paper I; Cheng 1972), the theory of nuclear reactions in solar flares was treated in detail and predictions were made as to the expected fluxes of gamma rays and high energy neutrons at earth from such reactions at the sun. Following the discovery by Chupp et al. we have reviewed and updated these calculations including more recent nuclear cross sections. By comparing the predicted emissions with the observations, we can show that the observed lines at 0.5, 2.2, 4.4 and 6.1 MeV are produced, respectively, by positron annihilation, deuterium deexcitation following neutron capture on hydrogen, and the deexcitation of the first nuclear levels of C^{12} and O^{16} . Furthermore, from the comparison of the calculated and observed line intensities we can deduce the spectrum of the accelerated particles at the sun independent of the assumed interaction model. The total number of accelerated particles required to produce the observed line emission, however, does depend on this model. In the subsequent treatment we shall use two limiting models. A thick-target model in which the accelerated particles move from the flare region downwards into the Sun undergoing nuclear interactions as they slow down in the solar atmosphere; and a thin target

model in which the spectrum of accelerated particles is not modified during the time in which the nuclear interactions take place. The latter model assumes that either the total path length traversed by the particles at the sun is small in comparison with their interaction length, or that the particle energy loss from ionization and nuclear interactions is just balanced by energy gains from acceleration.

We have recalculated the fluxes of various gamma ray lines expected from accelerated particle interactions in solar flares: at 0.511 MeV from positron annihilation, at 2.23 MeV from neutron capture on hydrogen and at 1.63, 1.99, 2.31, 4.43, 5.5 and 6.14 MeV from deexcitation of nuclear levels in C, O, N and Ne. These calculations are based on an ambient solar composition given by H:He:C:N:O = $1:10^{-1}:5.3 \times 10^{-4}:10^{-4}:9.2 \times 10^{-4}$ (Cameron 1967), and an accelerated particle population consisting of protons with spectrum

$$N(P) = P_0^{-1} \exp(-P/P_0). \quad (1)$$

Here P is rigidity, P_0 is a characteristic rigidity which we treat as a free parameter, and $N(P)$ is the total number of protons per unit rigidity. In the calculations $N(P)$ is normalized at the sun to 1 particle of rigidity greater than zero.

For the thick-target model, the yield of secondaries from a particular type of interactions is given by

$$Q_s = \eta \int_0^\infty dP N(P) \int_0^x dx' \sigma(P') \exp(-(x-x')/L), \quad (2)$$

where η is the number of target atoms per gram of solar material, σ is the cross section as a function of rigidity, and x and L are the

stopping range and nuclear interaction length of protons of rigidity P (both measured in g cm^{-2}). This yield has the units of secondaries per incident proton of rigidity greater than zero.

For the thin-target model, the instantaneous production rate of secondaries from the same type of interaction is

$$q_s = n c \int_0^{\infty} dP N(P) \beta \sigma(P) \quad (3)$$

where n is the number density of the ambient solar material in cm^{-3} , and $c \beta$ is the velocity of a proton of rigidity P . The units of q_s are secondaries per second per proton of rigidity greater than zero.

PHOTON PRODUCTION

Line emission at 0.511 MeV is produced from the annihilation of positrons. The principal source of positrons in solar flares are nuclear reactions of accelerated particles with the ambient solar atmosphere. These reactions produce π^+ mesons and a variety of radioactive isotopes which decay by positron emission. The main positron emitters, their formation reactions, threshold energies, half-lives and maximum positron energies are given in Table 1. Except for the reactions $N^{14} (p,n) O^{14}$ (e.g. Andouze, et al. 1967) and $N^{14} (p,d) C^{11}$ (Jacobs et al. 1972), the cross sections for these reactions were given in paper I. The resultant positron yields are given in Figures 1 and 2, for the thick- and thin-target models respectively.

The intensity of the 0.511 MeV line depends on the number of positrons that annihilate at the sun. For the thick-target model it

is reasonable to assume that all the flare produced positrons will ultimately annihilate at the sun. For the thin-target model, however, it is possible that a significant fraction of the positrons will escape from the sun before they annihilate. The determination of this fraction, however, is beyond the scope of the present paper and we defer the discussion on this for future research. For simplicity, in the subsequent calculations we assume that all flare produced positrons annihilate at the sun, but we keep in mind that this assumption may lead to too many 0.511 photons in the case of the thin-target model.

The annihilation radiation yield at 0.511 MeV also depends on the mode of positron annihilation. Positrons annihilate either directly with a free electron or in a bound state of positronium. In the latter case, the annihilations proceed from a 1S state leading to two 0.511 MeV photons, or from a 3S state leading to a 3-photon continuum. Since the 3-photon continuum does not contribute to line emission at 0.511 keV, and because the probability of forming the 3S state is 3 times that of the 1S state, positronium formation and its annihilation produces on the average only one 0.511 photon per positron as compared to two photons for free annihilation. This point was discussed in detail by Stecker (1969) for positron annihilation in interstellar space. However, in the much higher density and temperature of the solar atmosphere, we do not expect that positrons will annihilate from the 3S state of positronium, because the collision frequency of positronium with ambient electrons is sufficiently high to either dissociate the positronium or to cause a transition to the 1S state

before the annihilation of the 3S state. By allowing 2 photons per positron at the sun, the time-integrated 0.511 MeV line intensity at earth for the thick-target model is

$$F(0.511) = \frac{1}{2\pi R^2} [Q_s(\pi^+) + Q_s(C^{11}) + Q_s(N^{13}) + Q_s(O^{14}) + Q_s(O^{15})] \quad (4)$$

where the various Q_s 's are given in Figure 1. The units of F are photons cm^{-2} per proton of rigidity greater than zero. For the thin-target model we obtain an equation similar to equation (4), with F and Q_s replaced by the instantaneous rates ϕ and q_s . The units of ϕ are photons $\text{cm}^{-2} \text{sec}^{-1}$ per proton of rigidity greater than zero. The resultant 0.511 MeV photon fluxes are given in Figures 3 and 4, for the thick and thin-target models respectively.

Next we consider the 2.23 MeV line resulting from the deexcitation of deuterium following neutron capture on hydrogen. The principal neutron producing reactions and their cross sections were discussed in paper I and references therein. To these reactions we have added the reaction $N^{14}(p, n) O^{14}$ mentioned above which is important for low energy protons (< 15 MeV). The neutron producing reactions are summarized in Table 2. The total neutron yields for the thick- and thin-target models are then obtained by using the appropriate cross sections in equations (2) and (3). Having obtained the neutron yields, we have to consider the propagation of neutrons in the solar atmosphere, since 2.23 MeV photons are not produced if the neutrons escape from the sun or decay in the solar atmosphere.

Neutron propagation in the solar atmosphere is determined predominantly by scattering (elastic and inelastic) and capture by

protons. The total neutron-proton scattering cross section σ_s is essentially constant at 20 barns for neutron energies from 1 eV to 10^5 eV, and then drops to about 0.1 barns at 100 MeV (Hughes and Schwartz 1958). The capture cross section, is inversely proportional to velocity and is given by $\sigma_c \approx 2.2 \times 10^{-6} \beta^{-1}$, where σ_c is measured in barns and $c\beta$ is the velocity of the neutron. Since for all energies of interest $\sigma_s \gg \sigma_c$, the neutron mean free path in the solar atmosphere is determined principally by neutron-proton scattering. Using the columnar density of the solar atmosphere as given by Allen (1963), we find that a 10 MeV neutron moving radially outward from the sun will probably escape from the solar atmosphere before making even one collision if it is produced in a region of density less than 10^{17} cm^{-3} . This density corresponds to a depth of about 300 km below the base of the chromosphere. Since solar flares occur in the chromosphere or corona, it is reasonable to assume that for both interaction models, all upward moving neutrons are going to escape from the sun. The downward moving neutrons on the other hand decay or are captured, depending on whether the capture time is greater or smaller than the half-life of the neutrons. From the capture cross section σ_c , the capture time t_c is given by

$$t_c = (c\beta n \sigma_c)^{-1} \approx \frac{1.5 \times 10^{19}}{n(\text{cm}^{-3})} \text{ sec} \quad (5)$$

As can be seen, t_c is independent of energy and is inversely proportional to the density n of the region where the neutrons interact with the ambient medium. From the discussion above it follows that downward

directed neutrons probably will not collide with the ambient gas till they reach the photosphere where n is of the order 10^{17} cm^{-3} . Thus $t_c \approx 150$ seconds and since the half life of the neutron is 720 seconds, it follows that most of the neutrons will be captured before they decay. Furthermore, since the neutron capture occurs at a columnar depth of about 10^{24} cm^{-2} or 1.6 g cm^{-2} while the stopping range of a 2.2 MeV photon is about 25 g cm^{-2} , all the upward moving photons resulting from deuterium deexcitation will escape from the sun. Assuming isotropic production of neutrons in the interaction region, the 2.23 MeV line intensity at earth, for the thick- and thin-target model respectively are

$$F(2.23) = \frac{1}{4\pi R^2} \frac{1}{2} Q_S(n) \quad (6)$$

$$\phi(2.23) = \frac{1}{4\pi R^2} \frac{1}{2} q_S(n), \quad (7)$$

where $Q_S(n)$ and $q_S(n)$ are the total neutron yields as calculated from equations (2) and (3).

The calculations of the other intensities at 1.63, 1.99, 2.31, 4.43, 5.5 and 6.14 MeV in Figures 3 and 4 is straightforward. Unlike the 0.511 and 2.23 MeV lines, these emissions are prompt, i.e. the excited states or secondary products decay by photon emission in a time scale much shorter than any characteristic time of the flare process.

Line emission at 4.43 and 6.14 MeV results from the deexcitation of the first nuclear levels of C^{12} and O^{16} , respectively. The intensity of the 6.14 MeV line is the same as calculated in paper I. The

intensity of the 4.43 MeV line is about 50% greater than in paper I, because it is possible to produce $C^{12(4.43)}$ by the spallation of O^{16} , a process which was neglected in paper I. The calculations for this process given in Figures 3 and 4 are based on cross sections measured by Zobel et al. (1968).

Radiation at 2.31 MeV corresponds to the first nuclear level of N^{14} . The 2.31 MeV line is produced by the direct excitation of the first and second levels of N^{14} . The latter is at 3.94 MeV and it deexcites 96% of the time through the first level, thereby producing a 1.63 MeV photon in addition to the 2.31 MeV photon. In addition to direct excitation, the first level of N^{14} can also be populated by the decay of O^{14} which is produced by the reaction $N^{14}(p,n)O^{14}$. O^{14} beta decays 99.4% of the time to $N^{14}(2.31)$ and hence each beta decay is accompanied by a 2.31 MeV photon. As mentioned above, the 1.63 MeV line is formed by the deexcitation of $N^{14}(3.94)$. In addition, this line is also produced by the deexcitation of the first level of Ne^{20} . Finally the 1.99 MeV line results from the deexcitation of C^{11} which is formed from the spallation of C^{12} . The cross section for this process is given by Zobel et al. (1968).

The principal reason for showing the 1.99 MeV and the 2.31 lines is that for detectors of poor energy resolution these lines could in principle be confused with the deuterium deexcitation line. As can be seen from Figures 3 and 4, however, the $C^{11}(1.99)$ MeV line is negligible in comparison with the deuterium line. On the other hand, the 2.31 MeV line from N^{14} could compete with the 2.23 MeV line at

low P_0 's. If all the emission at ~ 2.2 MeV is from N^{14} , however, the intensities of the 4.43 MeV and 6.14 MeV lines should be about the same as that of the 2.2 MeV line. As will be discussed below, this was not the case for the August 4, 1972 event. Therefore, for this flare at least, we conclude that the 2.2 MeV line is produced almost entirely by neutron capture.

We have summarized in Table 3 the principal mechanism leading to line emission in the solar atmosphere. In addition to the lines given in Figures 3 and 4, we have listed in Table 3 lines at 5.2 MeV from O^{15} and N^{15} and at 7.12 MeV from O^{16} . From the cross sections of Zobel et al. (1968), the intensities of both these lines should be approximately 50% of the 6.14 MeV line intensity.

DISCUSSIONS

Let us now compare the results of our calculations with the observations of Chupp et al. (1972) for the August 4, 1972 flare. We defer the discussions on the August 7, 1972 observations, since the gamma rays from this flare were observed only after the flare maximum and hence they require a more detailed treatment of the time dependence of the gamma ray intensities.

In Figures 5 and 6, the shaded areas represent the time averaged ratios of the measured 0.5, 4.4 and 6.1 MeV line intensities to the measured 2.2 MeV line. The curves represent the calculated ratios as functions of the characteristic rigidity P_0 , for the thick-target model in Figure 5 and the thin-target model in Figure 6. As can be seen, the calculated 4.43 and 6.14 curves are strong functions of P_0 .

Therefore, the comparison of these ratios with the measurements allows us to deduce the value of the characteristic rigidity P_0 . We find that for both models P_0 has to be in the range 70 to 80 MV. This range of P_0 's should be compared with values of P_0 as obtained from charged particle observations near earth.

According to Bostrom et al. (1972) the peak proton intensities after the flare of August 4, 1972 were: $j(> 10 \text{ MeV}) = 10^6 \text{ cm}^{-2} \text{ sec}^{-1}$, $j(> 30 \text{ MeV}) = 2.6 \times 10^5 \text{ cm}^{-2} \text{ sec}^{-1}$, and $j(> 60 \text{ MeV}) = 8 \times 10^4 \text{ cm}^{-2} \text{ sec}^{-1}$. From these intensities we can deduce the local proton density u in the interplanetary medium. If $u(P) \propto \exp(-P/P_0)$ and if the protons are non-relativistic

$$u(> P) = j(> P) (mc/e) (P+P_0)^{-1}. \quad (8)$$

From equation (8) and the integral intensities $j(> P)$ given above, we can calculate values of $u(> P)$ for various P_0 's. For $P_0 = 65 \text{ MV}$ we obtain proton densities as follows:

$$u(> 10 \text{ MeV}) = 1.53 \times 10^{-4}, \quad u(> 30 \text{ MeV}) = 2.67 \times 10^{-5}, \quad \text{and} \quad u(> 60 \text{ MeV}) = 6.13 \times 10^{-6}.$$

These numbers are plotted in Figure 7 as functions of P . The straight lines are exponentials in rigidity with $P_0 = 60 \text{ MV}$ and $P_0 = 70 \text{ MV}$ and they bracket the observed proton densities. The charged particle observations at the peak of the proton event are therefore consistent with a characteristic rigidity of about 60 to 70 MV. Furthermore, this characteristic rigidity remains essentially the same for the remainder of the particle event (J. King, private communication).

The similarity between the proton spectrum as observed near earth and the proton spectrum at the sun as deduced from the gamma ray observations, seems to imply that, at least for the August 4, 1972 flare, both the escape of particles from the flare region and their propagation in the interplanetary medium are essentially independent of energy.

Let us now calculate the total number of protons at the sun. In the case of the thick-target model this calculation is independent of the ambient density n but requires the knowledge of the time-integrated photon flux from the flare. According to Chupp et al. (1972) the average intensities of the 2.2 MeV line from 0626 UT to 0632 UT on August 4, 1972 was $0.22 \text{ photons cm}^{-2} \text{ sec}^{-1}$ and thus the total photon flux in the 6 minute time interval was $80 \text{ photons cm}^{-2}$. This is only a lower limit because OSO-7 went into earth eclipse at 0632 before the termination of the gamma ray event. The total gamma ray flux, however, was probably not much larger, since as indicated by the microwave data (Toyokawa observatory, private communication), the acceleration of the charged particles probably ceased at 0635 UT, 3 minutes after the eclipse of OSO-7.

For a flux of $80 \text{ photons cm}^{-2}$ and P_0 ranging from 60 MV to 70 MV, we find from Figure 3 that $N(> P)$ is between 1.4 and 6×10^{33} . These numbers should be compared with the number of protons released from the flare based on measurements of the proton flux near earth. This number can be obtained from the local densities shown in Figure 7 if we assume that the particles fill some volume V in the interplanetary

medium to that density. A conservative estimate of this volume would be to assume that it is a cone of opening angle 30° with vertex at the sun and height 1.5 A.U. This is consistent with the fact that the August 4 flare was located at 15°N latitude on the sun and that some charged particles were observed on the Pioneer 10 space probe at 2 A.U. from the sun (B. J. Teegarden, private communication). The volume V is therefore $\sim 10^{39} \text{ cm}^3$ and from Figure 7, $N(> P)$ is 7×10^{35} and 1.5×10^{36} for P_0 equal 70 MV and 60 MV respectively. When compared with the values of $N(P > 0)$ deduced above from the gamma ray observations for the thick-target model, we see that possibly not more than about 1% of the flare accelerated protons could have escaped downward into the sun. However, we should note that this conclusion is strongly dependent on our estimate of the total number of protons at the sun based on the local proton observations. Clearly a more detailed understanding of the source function of flare protons in the interplanetary is required.

In case of the thin-target model, the instantaneous photon flux at earth directly determines the emission measure at the sun, i.e. the product $nN(P > 0)$. From Figure 4 we find that the observed flux of $0.22 \text{ photons cm}^{-2} \text{ sec}^{-1}$ implies that nN is 1 to $2 \times 10^{45} \text{ cm}^{-3}$ for P_0 ranging from 70 MV to 60 MV. Then using the values of $N(P > 0)$ as deduced from the proton flux near earth, we get that n is 1.5 to $3 \times 10^9 \text{ cm}^{-3}$. As before, we note that this density is subject to the uncertainty in the total number of protons at the sun obtained from the local observations.

Let us finally evaluate the total energy in the flare accelerated protons that produce gamma rays at the sun. For the spectrum given in equation (1) and nonrelativistic protons, the average proton energy is P_0^2/Mc^2 . Therefore, for the thick-target model, the energy in the 1.4 to 6×10^{33} protons as deduced above is 1.2 to 3.7×10^{28} ergs.

For the thin-target model, both the instantaneous gamma ray production rate and the instantaneous proton energy loss rate depend on the product of the ambient density n and the total number of protons at the sun. The ratio of these two rates, therefore, is independent of both n and N and depends only on the spectrum of the accelerated particles, i.e. P_0 in our calculations. This point was first made by Lingelfelter (1969). For the proton distribution in equation (1) normalized to 1 proton of rigidity greater than zero, the instantaneous energy loss rate W to ionization, excitation and nuclear interactions in ambient hydrogen of unit density is given in Table 4. As can be seen, for P_0 's between 60 to 70 MV, W is very closely equal to 1.7×10^{-18} ergs sec^{-1} . Using the values of Nn given above, we see that gamma ray production by flare accelerated protons is accompanied by the dissipation of 1.7 to 3.4×10^{27} ergs sec^{-1} . For the time interval of 6 minutes during which gamma rays were observed, the total dissipated energy is 0.6 to 1.2×10^{30} ergs.

This energy is comparable to the total of $\sim 2 \times 10^{30}$ ergs emitted in H-alpha by the flare of August 4, 1972 (H. Zirin, private communication) and is consistent with the suggestion of Gordon (1954) that the

optical energy from flares results from ionization losses of accelerated particles. On the other hand, in the thick-target model, the ionization losses of the gamma-ray producing protons is only a few percent of the observed optical energy; in this case additional energy loss may be expected from electrons.

REFERENCES

- Allen, C. W. 1963, Astrophysical Quantities (Athlone Press, London).
- Audouze, J., Ephere, M., and Reeves, H. 1967, High-Energy Nuclear Reactions in Astrophysics, ed. by B.S.P. Shen, W. A. Benjamin, New York, 255.
- Bostrom, C. O., Kohl, J. W., and McEntire, R. W. 1972, The solar proton flux - August 2-12, 1972 (The Johns Hopkins University, Applied Physics Laboratory, Silver Spring, Maryland).
- Cameron, A.G.W. 1967, Origin and distribution of elements, ed. by L. H. Ahrens (Pergamon Press, London).
- Cheng, C. C. 1972, Space Science Review, 13, 3.
- Chupp, E. L., Forrest, D. J., Higbie, P. R., Suri, A. N., Tsai, C., and Dunphy, P.P. 1972, Nature (in press).
- Gordon, I. M. 1954, Dokl. Akad. Nauk SSSR, 96, 813.
- Hughes, D. J. and Schwartz, R. B. 1958, Neutron Cross Sections (Brookhaven National Laboratory, Upton, New York).
- Jacobs, W.W., Bodansky, D., Cameron, J.M., Oberg, D., and Russo, P. 1972, Bull. Amer. Phys. Soc. 17, 479.
- Lingenfelter, R. E. and Ramaty, R. 1967, High-Energy Nuclear Reactions in Astrophysics, ed. by B.S.P. Shen, W. A. Benjamin, New York, 99.
- Lingenfelter, R. E. 1969, Solar Physics, 8, 341.
- Stecker, F. W. 1969, Astrophys. Space Sci., 3, 479.
- Zobel, W., Maienschein, F. C., Todd, J. H., and Chapman, G. T. 1968, Nuclear Science and Engineering, 32, 392.

FIGURE CAPTIONS

- Figure 1 - Yield of positron emitters at the sun for the thick-target model.
- Figure 2 - Production rate of positron emitters at the sun for the thin-target model.
- Figure 3 - Time integrated photon fluxes at earth in the thick-target model.
- Figure 4 - Instantaneous photon fluxes at earth in the thin-target model.
- Figure 5 - Relative line intensities for the thick-target model
- Figure 6 - Relative line intensities for the thin-target model.
- Figure 7 - Proton densities in the interplanetary medium from local particle measurements.

TABLE 1

Positron Emitters

β^+ Emitter and Decay Mode	Maximum Positron Energy, Mev	Half-life (min)	Production Mode	Threshold Energy, Mev
$C^{11} \rightarrow B^{11} + \beta^{+} + \nu$	0.97	20.5	$C^{12}(p, pn)C^{11}$	20.2
			$N^{14}(p, 2p2n)C^{11}$	13.1
			$N^{14}(p, \alpha)C^{11}$	2.9
			$O^{16}(p, 3p3n)C^{11}$	28.6
$N^{13} \rightarrow C^{13} + \beta^{+} + \nu$	1.19	9.96	$N^{14}(p, pn)N^{13}$	11.3
			$O^{16}(p, 2p2n)N^{13}$	5.54
$O^{14} \rightarrow N^{14} + \beta^{+} + \nu$	1.86	1.18	$N^{14}(p, n)O^{14}$	6.4
$O^{15} \rightarrow N^{15} + \beta^{+} + \nu$	1.73	2.07	$O^{16}(p, pn)O^{15}$	16.54

TABLE 2
Neutron Producing Reactions

Reaction	Threshold Energy Mev/Nucleon
$H^1 (p, n\pi^+) H^1$	292.3
$He^4 (p, pn) He^3$	25.9
$He^4 (p, 2pn) H^2$	32.8
$He^4 (p, 2p2n) H^1$	35.6
$C^{12} (p, n\dots)$	19.8
$N^{14} (p, n\dots)$	6.3
$O^{16} (p, pn\dots)$	16.5
$Ne^{20} (p, pn\dots)$	17.7

TABLE 3

Gamma Ray Line Emission Mechanisms

Photon Energy (MeV)	Origin	Production Mode
0.511	Positron Annihilation	Table 1
2.23	Deuterium deexcitation following neutron capture	Table 2
1.63	^{20}Ne (1.63) deexcitation	^{20}Ne (p,p') ^{20}Ne (1.63)
	^{14}N (3.94) \rightarrow ^{14}N (2.31) deexcitation	^{14}N (p,p') ^{14}N (3.94)
2.31	^{14}N (2.31) deexcitation	^{14}N (p,p') ^{14}N (2.31)
		^{14}N (p,p') ^{14}N (3.94) \rightarrow ^{14}N (2.31)
4.43	^{12}C (4.43) deexcitation	^{14}N (p,n) ^{14}O \rightarrow ^{14}N (2.31) ^{12}C (p,p') ^{12}C (4.43) ^{16}O (p,) ^{12}C (4.43)
5.2	^{15}O (5.20) deexcitation	^{16}O (p,) ^{15}O (5.20)
	^{15}N (5.28) deexcitation	^{16}O (p,) ^{15}N (5.28)
6.14	^{16}O (6.14) deexcitation	^{16}O (p,p') ^{16}O (6.14)
7.12	^{16}O (7.12) deexcitation	^{16}O (p,p') ^{16}O (7.12)

TABLE 4

Energy loss rate of the proton distribution in
Eq. (1) in solar material of $n = 1 \text{ cm}^{-3}$

<u>P_o (MV)</u>	<u>$W(\text{erg sec}^{-1})$</u>
20	2×10^{-18}
30	2×10^{-18}
40	1.9×10^{-18}
60	1.8×10^{-18}
80	1.6×10^{-18}
100	1.5×10^{-18}
120	1.4×10^{-18}
200	1.2×10^{-18}
300	1.1×10^{-18}

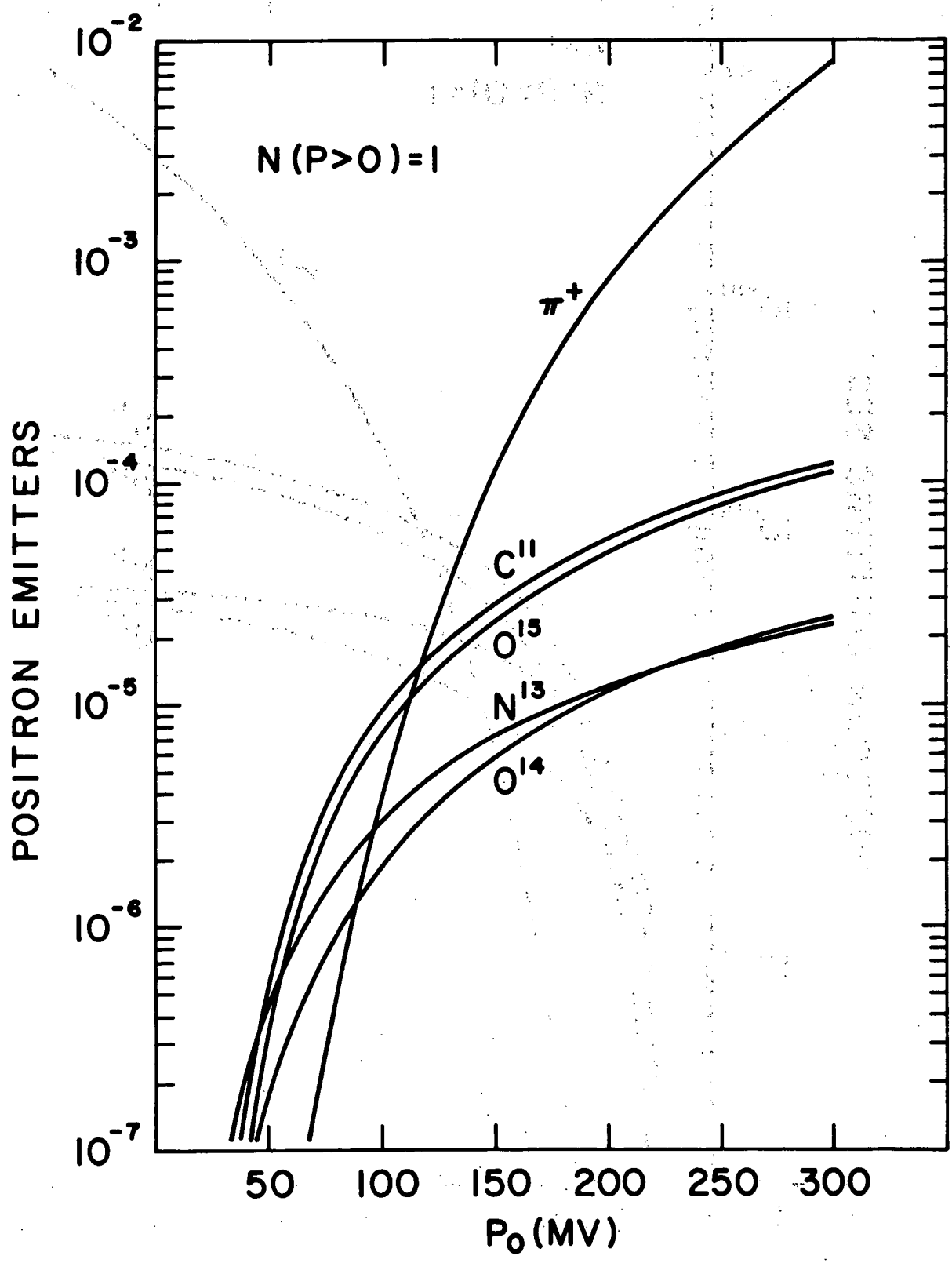


Figure 1

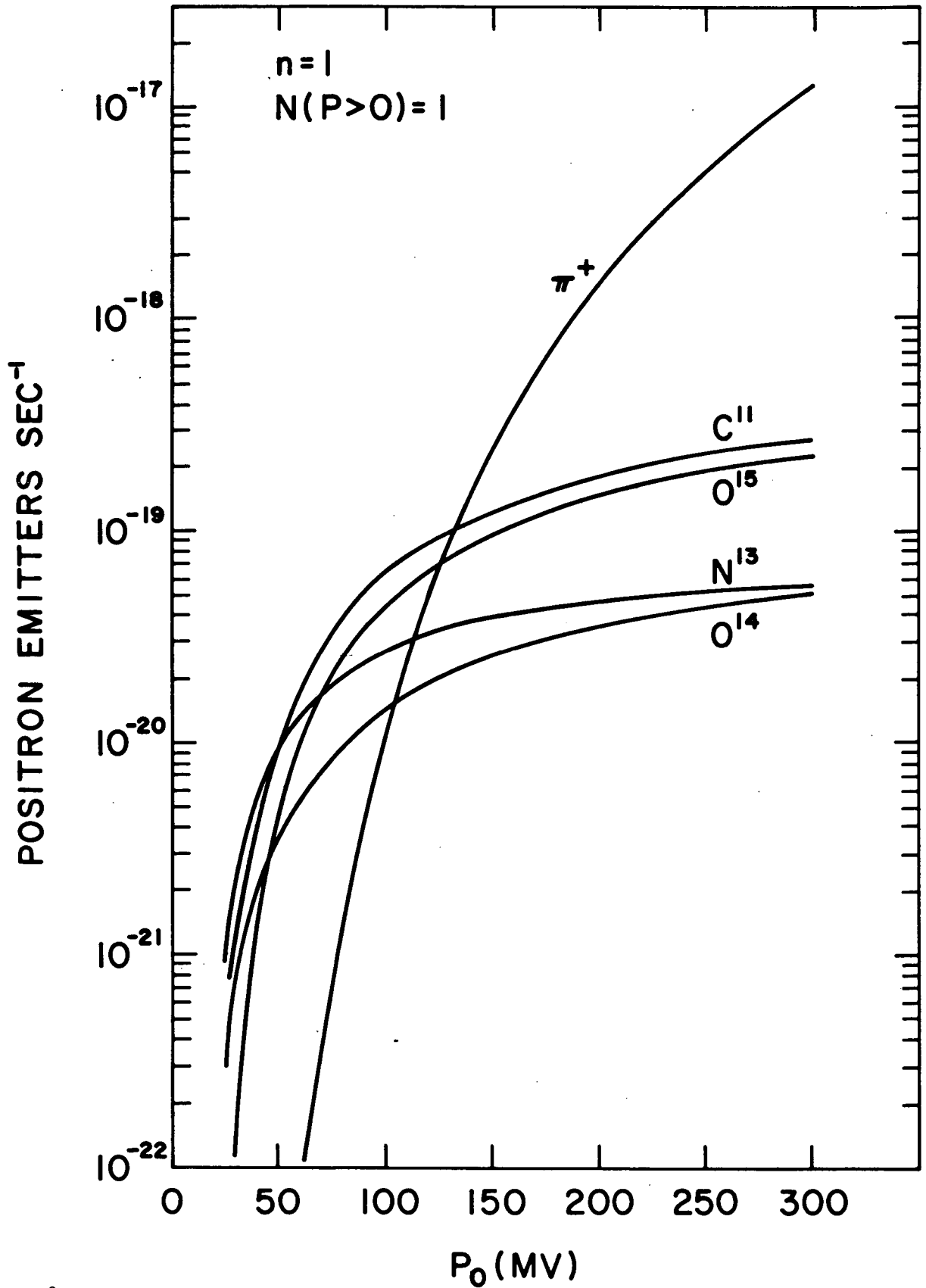


Figure 2

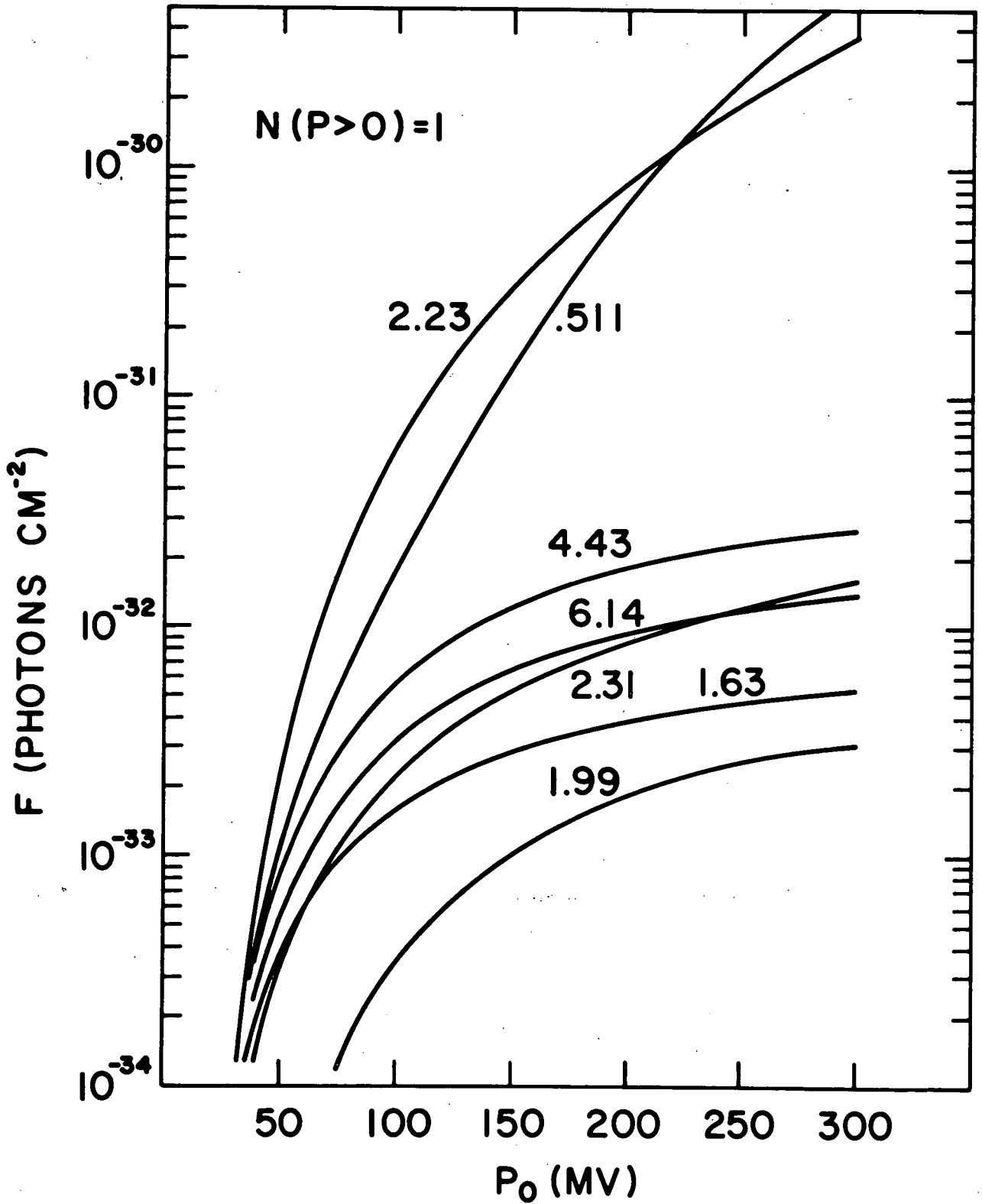


Figure 3

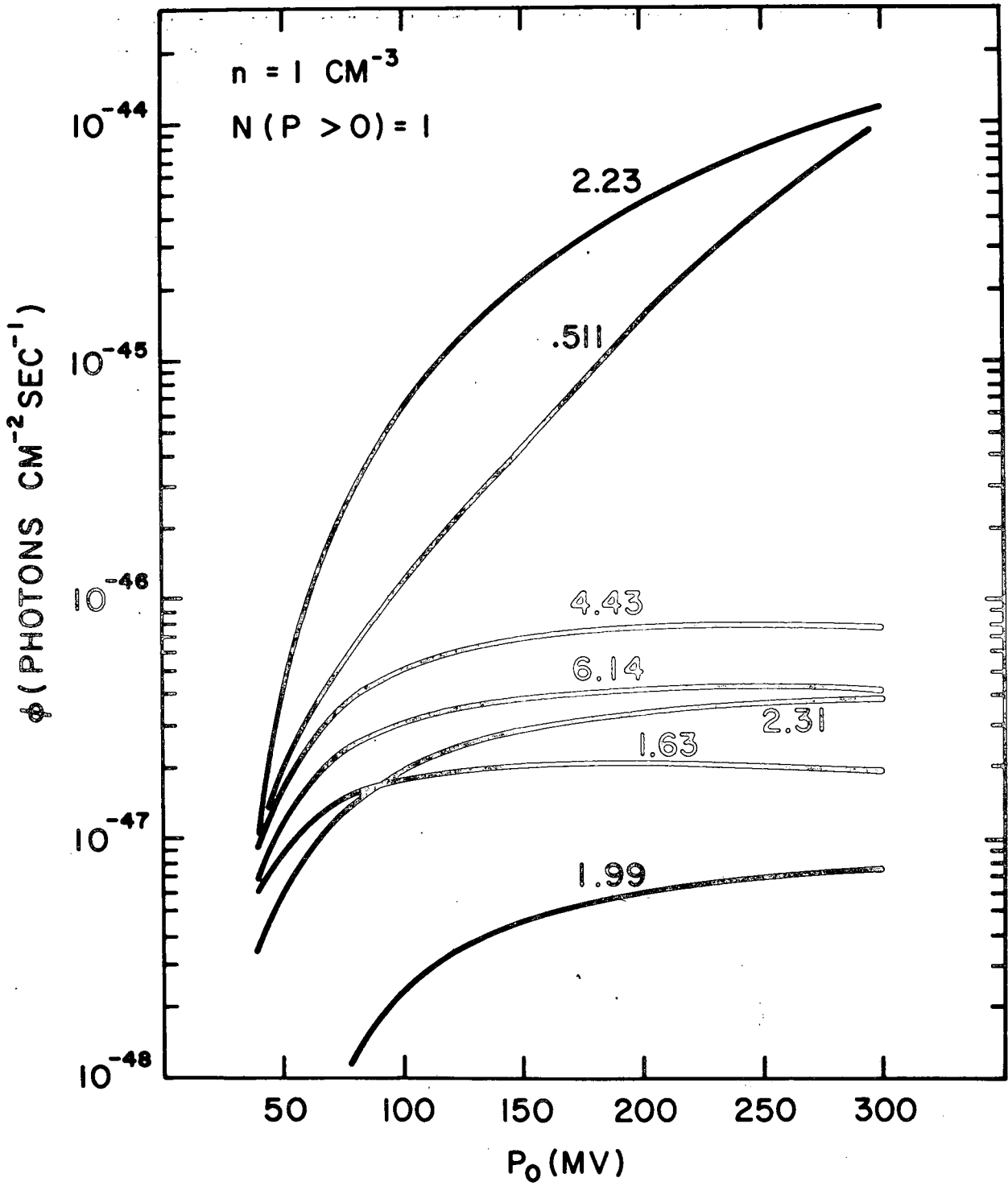


Figure 4

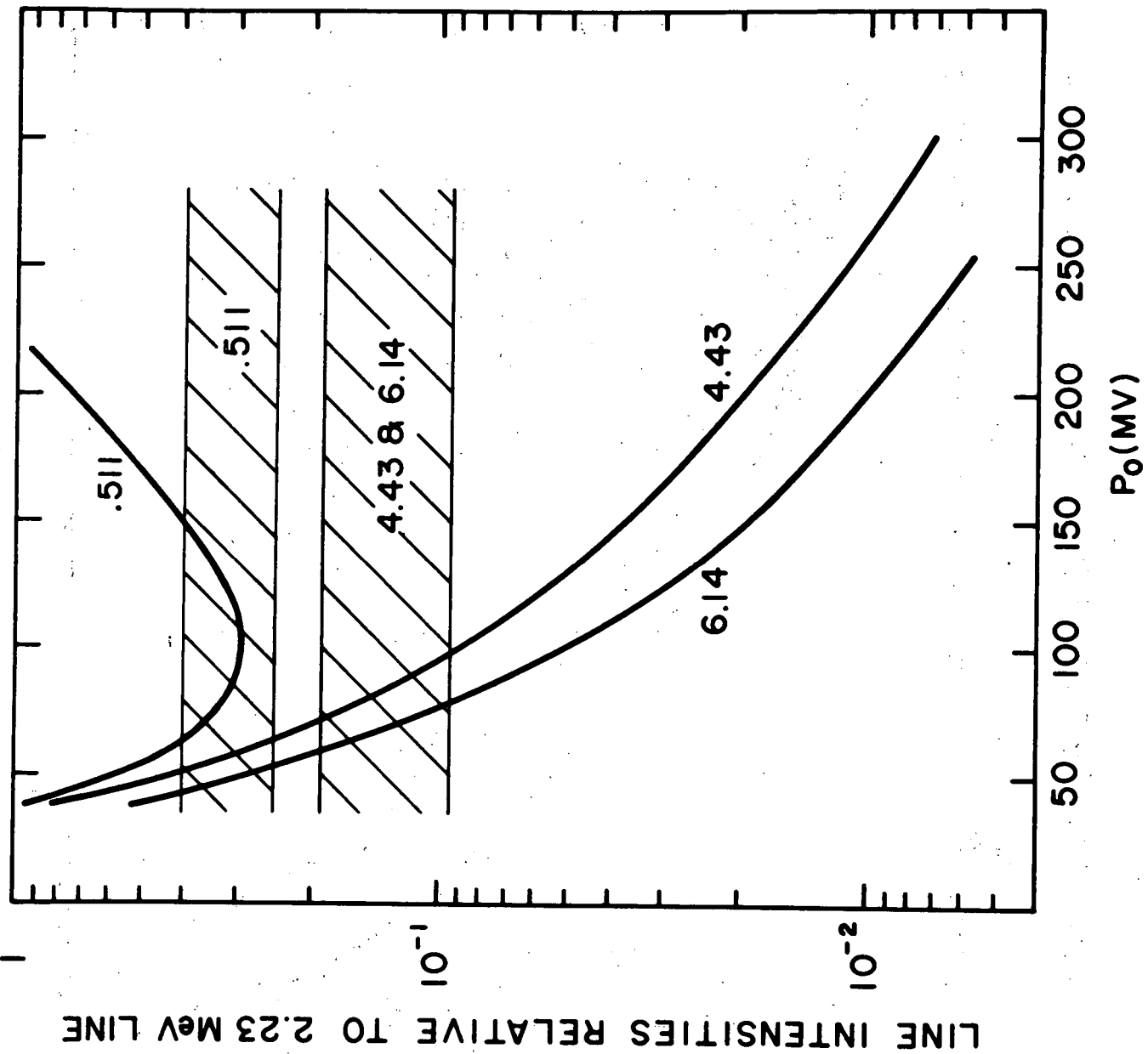


Figure 5

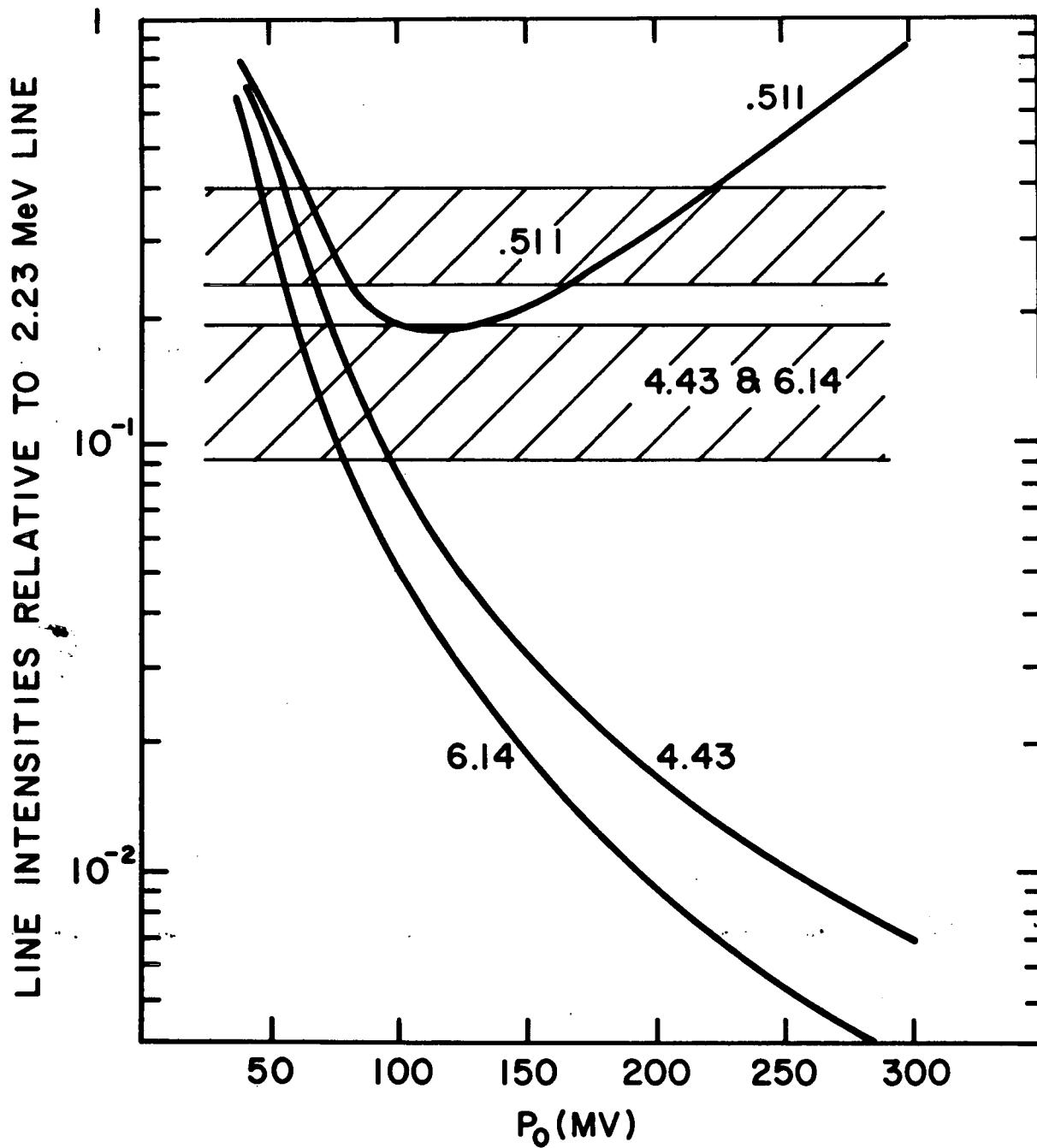


Figure 6

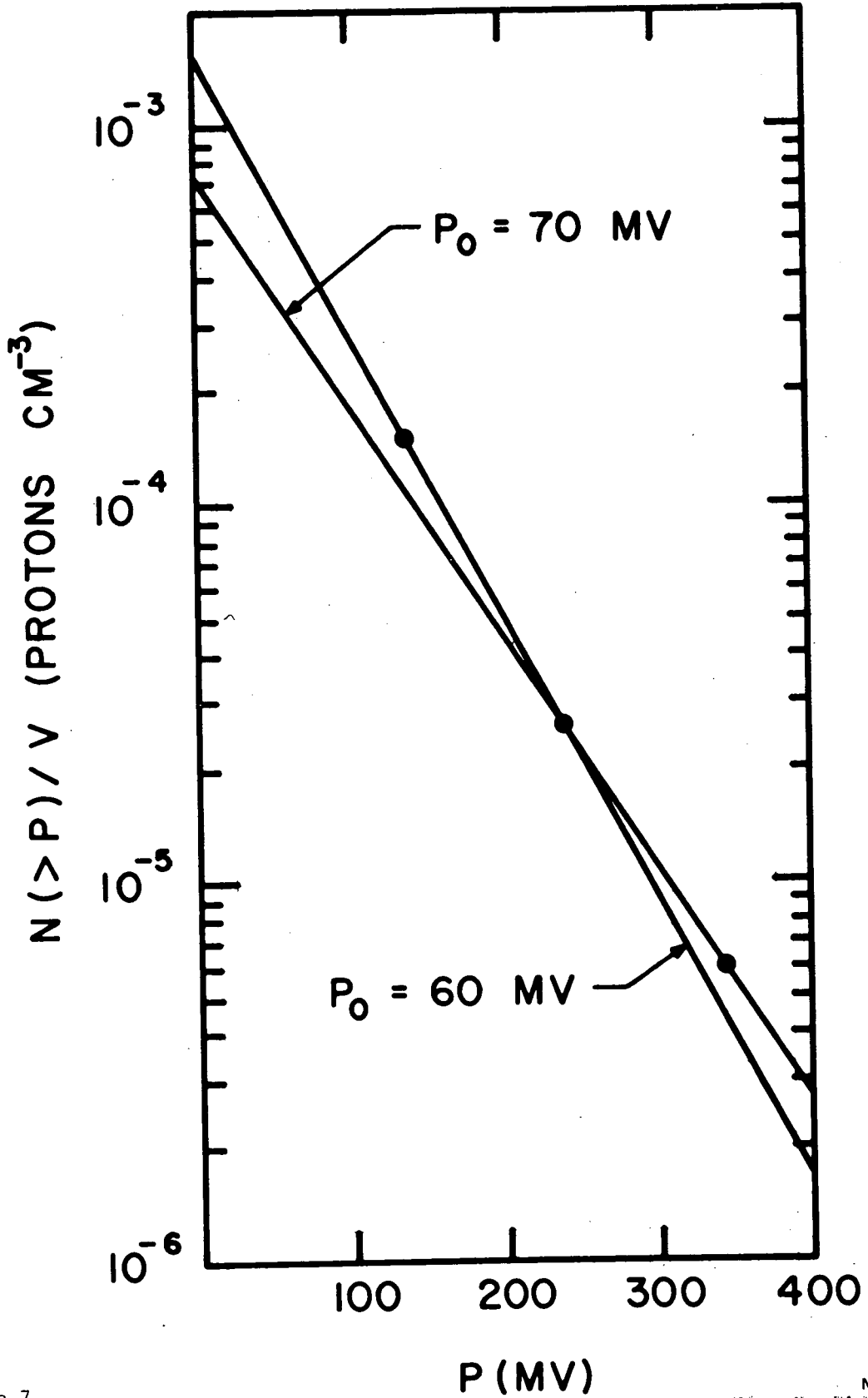


Figure 7